Hypochlorite scavenging activity of cerium oxide nanoparticles

Gerardo Pulido-Reyes[1], Soumen Das[2], Francisco Leganés[1], Sueli O. Silva[3], Shu-Pao Wu[6], Francisca William Self[5], Fernández-Piñas[1], Roberto Rosal[6,*], Sudipta Seal[2,7,*]

1 Departamento de Biología, Facultad de Ciencias, Universidad Autónoma de Madrid, E-28049, Spain
2 Advanced Materials Processing and Analysis Center, NanoScience and Technology Center, Materials Science and Engineering, University of Central Florida, Orlando, FL 32816, USA
3 Departamento de Ciências Básicas da Saúde, Universidade Estadual de Maringá, 87020-900 Maringá, PR, Brazil.
4 Department of Applied Chemistry, National Chiao Tung University, Hsinchu, Taiwan 300, Republic of China.
5 Burnett School of Biomedical Science, College of Medicine, University of Central Florida, USA.
6 Departamento de Ingeniería Química, Universidad de Alcalá, E-28871, Alcalá de Henares, Madrid, Spain
7 College of Medicine, University of Central Florida, USA

* Corresponding authors: roberto.rosal@uah.es, sudipta.seal@ucf.edu

Abstract

In this report, we provide evidence that specific synthesis of cerium oxide nanoparticles can scavenge hypochlorite anion, which is a strong extracellular oxidant involved in the inflammatory processes. The scavenging process takes place by a surface reaction involving the evolution of oxygen and the reduction of Ce^{4+} to Ce^{3+}.

Reactive oxygen species (ROS) or oxidants are associated with different diseases and aging [1]. Among them, HOCl/ClO^- is a strong oxidant produced by activated neutrophils and monocytes. Activated neutrophils or monocytes produce myeloperoxidase, which reacts with hydrogen peroxide and chloride ions giving rise to hypochlorous acid, HOCl, a strong nonselective oxidant [2,3]. HOCl production is part of the host defense mechanism against microorganisms; however, these properties may involve the risk of tissue damage through the same processes used in the destruction of invading microorganisms. In fact, neutrophil oxidants have been shown to be implicated in the tissue injury associated with inflammatory diseases, including respiratory distress, ischemia–reperfusion injury, acute vasculitis, arthritis, inflammatory bowel diseases, and glomerulonephritis [4].

Antioxidant and some natural compounds have been shown to scavenge hypochlorite such as flavonoids, polyphenols or hydroxycinnamic acids [5–8]. Cerium oxide nanoparticles (CNPs) have recently been shown as an inorganic regenerative antioxidant in biological systems [9]. CNPs are characterized by a complex redox chemistry due to the presence of Ce^{3+} atoms accompanying oxygen vacancies which are surrounded by Ce^{4+} atoms [10]. It has been reported that CNPs display superoxidedismutase mimetic activity [9], catalase mimetic activity [11] and the capacity to scavenge nitric oxide radicals [12]. Therefore, CNPs could potentially be used in biomedicine to fight against oxidative stress.

Although there are studies which describe the antioxidant properties of CNPs [13,14], in particular superoxide radical, hydrogen peroxide, hydroxyl radical and nitric oxide/peroxynitrite radical, in general, the antioxidant activity of these nanoparticles has been measured indirectly by intermediaries [15,16] and the reactions and subproducts which are generated after the interaction between CNPs and free radicals have not been fully characterized. Moreover, until now, there has been no evidence that CNPs can scavenge HOCl/ClO^-. A complete knowledge of the interaction of all physiological compounds with CNPs is completely necessary before assessing the massive use of CNPs in biomedical applications. In this study, we investigated whether CNPs are capable of scavenging HOCl/ClO^- and explored the reaction mechanism by which this phenomenon occurs. The proposed scavenging method which is shown here improves the speed of scavenging reaction of this particular ROS in comparison with already published articles [17] and clearly shows that it is effective in an in vitro cell model.

It is well established that physicochemical properties of CNPs govern the catalytic activity. Therefore, in this study we have selected four different CNPs (synthesized or commercially available) which have been used in previous studies and named as CNP1 [18], CNP2 [19], CNP3 [12] and CNP4 [18]. Physicochemical properties of the four nanoparticles were thoroughly analyzed and summarized in Table 1. In particular, size, morphology, agglomeration status, surface charge and surface Ce^{3+}/Ce^{4+} were measured. These above mentioned parameters were investigated as catalytic activity of CNPs can be highly influenced by these parameters as follows: (1) size – directly correlated with surface area and density of active site; (2) morphology and crystallinity – surface energy and stability of the particles; (3) agglomeration status – directly correlated with available surface for catalytic activity; (4) surface Ce^{3+}/Ce^{4+} – the presence of both surface oxidation states at nanoscale make nanoparticles catalytically active, CNPs with higher Ce^{3+}/Ce^{4+} scavenge more superoxide radicals whereas lower Ce^{3+}/Ce^{4+} scavenge hydrogen peroxide and nitric oxide radicals [20]. The size and morphology of particles were assessed using High Resolution Transmission Electron Microscopy (HRTEM). They were all round-shaped with particle nominal size in the 3–20 nm range. The selected area electron diffraction (SAED) pattern revealed that all four particles were crystalline (HRTEM images and SAED pattern are shown in the supplementary document, ESI Fig. S1).

Table 1. Physicochemical characterization of CNPs.

Sample	Surface Ce^{3+}(%)	Shape	ζ-potential (mV)	Effective diameter (DLS, nm)
CNP1	27	round	52.3 ± 0.5	50.8 ± 0.9
CNP2	40	round	56.5 ± 1.4	58.8 ± 0.8
CNP3	30	round	46.0 ± 2.5	9.4 ± 2.1
CNP4	57	round	18.6 ± 0.6	30.8 ± 2.8

TheEffective diameter and zeta-potential of the CNPs suspensions were measured by dynamic light scattering (DLS) and electrophoretic light scattering, respectively (Zetasizer Nano ZS from Malvern Instruments). The data, obtained for 1 mM suspensions in high purity water at pH 7.5, are shown in Table 1. X-ray photoelectron spectroscopy data were collected for Ce $3d_{5/2}$ using 5400 PHI ESCA spectrometer (Mg-Kα X-radiation (1253.6 eV) at a power of 350 W was used during the data collection). Surface Ce^{3+}/Ce^{4+} was calculated as discussed in our previous publication [21].

These well characterized nanoparticles were investigated for ClO^- scavenging activity. The nanoparticle suspensions (from 0.1 to 4 mM) were incubated for 60 min with freshly prepared hypochlorite solutions (5 mM, pH 9.0 ± 0.2). Then, the particles were separated by centrifugation (23 000g, 5 min). The

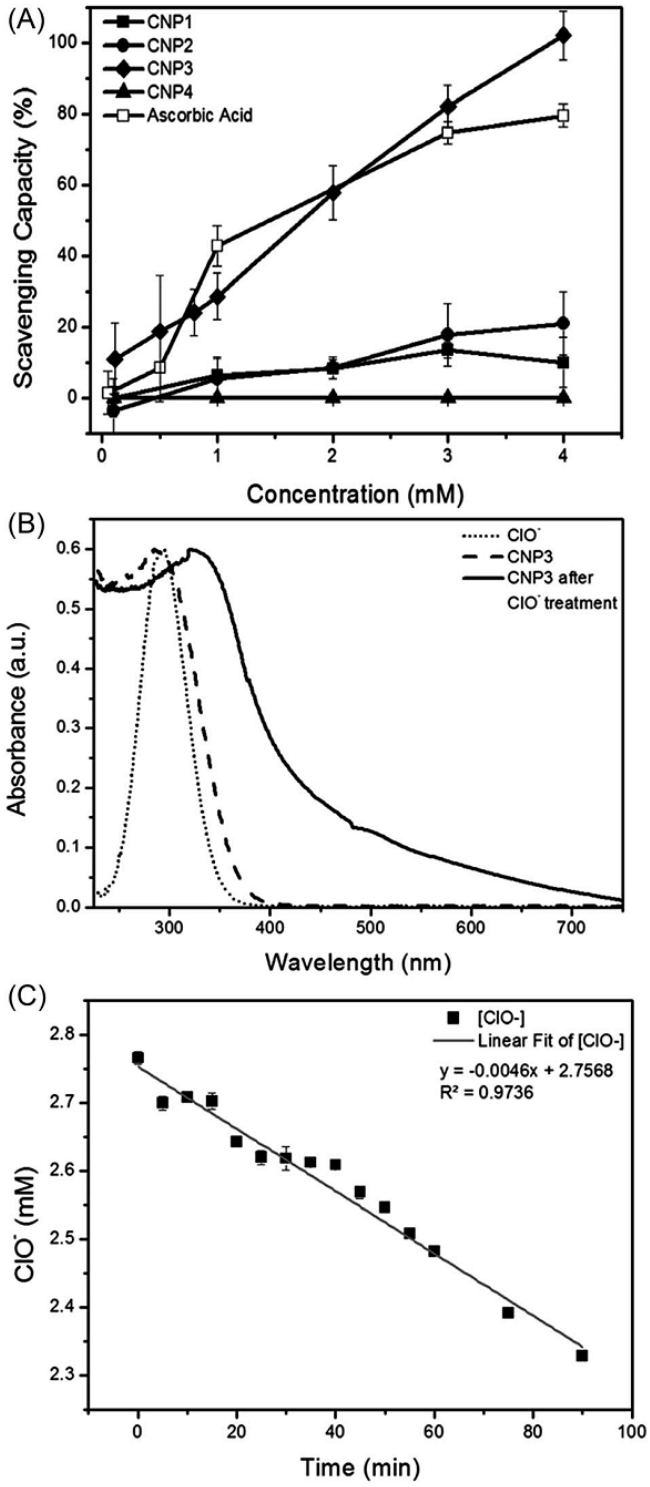

Figure 1. (A) ClO^- scavenging activity of CNP determined from catalase inactivation measurements. (B) UV-vis spectra showing the interaction of CNP3 and ClO^-. (C) Kinetics of ClO^- depletion by CNP3.

amount of ClO^- (at the working pH, hypochlorous acid, pKa 7.5, is 97% dissociated) in the supernatant, which decreased due to the scavenging activity of CNPs, was tracked by measuring the inactivation of catalase. The method followed the procedure described by Aruoma and Halliwell [22] with minor variations. The scavenging activity was evaluated by measuring the

decrease in absorbance of catalase at 404 nm using microplate readings (FLUOstar Omega microplate reader, BMG LABTECH, Germany). The data are shown in Fig. 1A for the tested CNPs and the reference antioxidant compound ascorbic acid [23]. Scavenging activity (%) was calculated using the following formula:

$$Scavenging\ activity\,(\%) = \frac{(C_x - C_{t2})}{(C_{t1} - C_t)} 100 \quad (1)$$

where C_{t1} is the catalase absorbance (measured at 404 nm) without ClO^- (intact catalase); C_{t2} is the catalase absorbance in the presence of ClO^- (degraded catalase) and C_x is the catalase absorbance with ClO^- which was previously in contact with CNPs or ascorbic acid.

The data show that CNP3 has strong ClO^- scavenging activity, with reaction extents comparable to the same concentration of ascorbic acid. The interaction of CNP3 with ClO^- was revealed by absorption spectroscopy. The absorption spectra of CNP3, recorded using a Perkin Elmer Lambda 750S instrument, show a shift in the absorption peak from 300 to 322 nm in CNP exposed to ClO^- (60 min), separated by centrifugation and carefully washed three times before recording the spectrum (Fig. 1B). A similar phenomenon was found with CNP2 (see ESI Fig. S2). Absorbance values at wavelengths 298 and 252 nm are the characteristic UV-Vis absorbance for Ce^{4+} and Ce^{3+}, respectively [24]. Fig. 1B clearly indicates that there is a shify in CNPs surface oxidation state from Ce^{4+} to Ce^{3+} after reacting with ClO^-. The disappearance of ClO^- from CNPs suspensions could not be attributed to its mere adsorption on the nanoparticle surface. A kinetic study was undertaken in mixtures of ClO^- and CNPs (5 mM) by following the evolution of hypochlorite concentration with time. The UV absorbance at 292 nm (molar absorptivity 350 M^{-1} cm^{-1}) was measured to estimate the concentration of the ClO^- on the supernatant of centrifuged samples [25]. The corresponding data are shown in Fig. 1C for CNP3. We selected CNP3 as CNP3 showed highest ClO^- scavenging activity. A Langmuir kinetics assuming surface equilibrium yields the following expression [26]:

$$r = \frac{k\,K\,C}{1 + K\,C} \quad (2)$$

where k is the rate of reaction of adsorbed species, K the adsorption equilibrium constant and C is the concentration of ClO^-. Given the relatively low concentration used, the zero order kinetics depicted in Fig. 1C points towards a high adsorption constant of ClO^- on CNP.

In order to better understand the interaction between ClO^- and CNP, XPS analysis was performed to further confirm the change in Ce^{3+}/Ce^{4+} on the surface of the nanoparticles seen in UV-Vis data. CNP3 was washed three times with distilled water after 60 min treatment with 5 mM ClO^-, to make sure there was no free ClO^-. The Ce $3d_{5/2}$ spectra recorded (Fig. 2A and B) showed a significant increase in surface Ce^{3+} (12%) after interaction of CNP3 with ClO^- for 60 min at pH 9.0. The presence of chloride on CNP3 surface after treatment with ClO^- is also apparent (Fig. 2C). The shift in Cl $2p_{3/2}$ spectrum compared to $CeCl_3$ may signify a complex formation on the surface of the nanoparticles rather than formation of $CeCl_3$ on the surface. Based on these results, we hypothesized the following reaction by means of which ClO^- is depleted by interaction with CNP3:

$$Ce^{4+} + 2ClO^- \rightarrow Ce^{3+} + 2Cl^- + O_2 \quad (3)$$

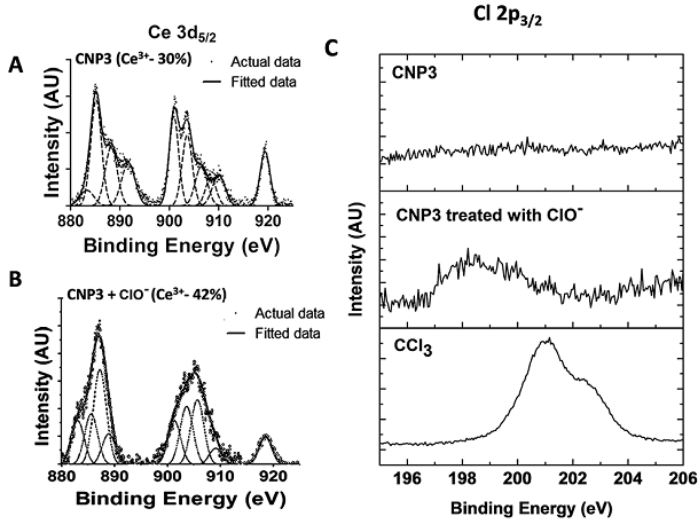

Figure 2. The chemical property of the CNP3 after treatment with ClO^-. (A) and (B) show a significant change in Ce $3d_{5/2}$ XPS spectrum after treatment with ClO^-. (C) Shows Cl $2p_{3/2}$ spectra of CNPs, CNPs treated with ClO^- and $CeCl_3$ ($CeCl_3$ was used as reference) and indicates the presence of Cl on the surface of the nanoparticles after reaction of ClO^-.

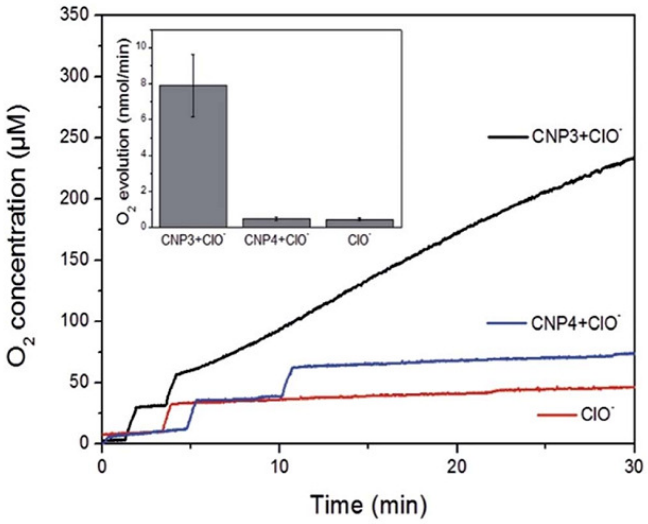

Figure 3. Oxygen evolution for CNP in contact with ClO^-.

The reaction accounts for the formation of chlorine–metal bonds due to chloride adsorption on the positively charged surface and should be accompanied by a release of oxygen. In order to prove that ClO^- decomposes as indicated, we performed direct measurements of oxygen evolution using a Clark-type oxygen electrode. The experiments were performed at 25 °C under constant stirring (0.1 g) using a Hansatech apparatus (Kings Lynn, Norfolk, UK) with 1 μM CNPs and 5 mM of ClO-.

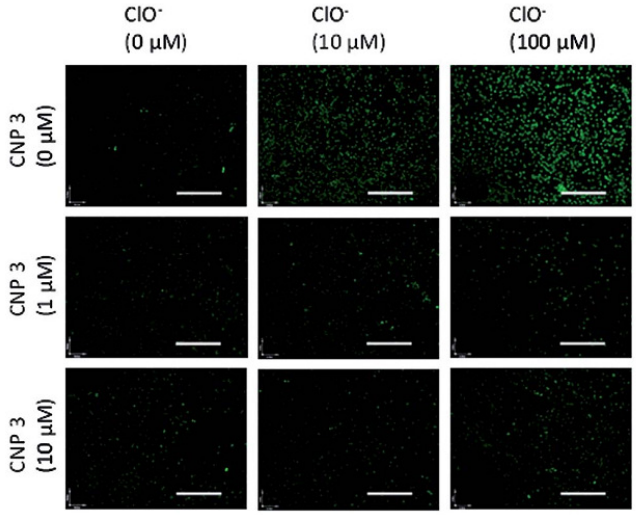

Figure 4. Scavenging of ClO^- by CNP3 in vitro RAW cell culture model. Pretreatment with 1 μM CNP3 able to scavenge the most of the ClO^- (comparable to control); scale bar 50 mm.

The results are shown in Fig. 3 and revealed a significant evolution of oxygen for CNP3 (CNP4 and ClO^- without nanoparticles are also shown for comparison), which amounted to 8 nmol min^{-1} or 0.32 mol O_2 mol per CNP per h. There was no evidence of oxygen release when nanoparticle or ClO^- alone was added (ESI Fig. S3). Lastly, we explored if CNP could scavenge ClO^- in the cellular environment. RAW 264.7 cells culture was selected as in vitro model and boron dipyrromethene-based fluorometric probe, HCS, was used to detect the ClO^- [27]. Data are shown in Fig. 4. Confocal images clearly indicate that concentration of ClO^- in the cells pretreated with CNP3 is comparable to the control. 1 μM concentration of CNP3 was sufficient to scavenge the ClO^- to its basal level (control) in the RAW cell model. Fluorescence intensity was also measured using Image J software and is shown in ESI Fig. S4.

Conclusions

The higher activity of CNP3 in comparison with the other tested nanoparticles is apparent from the data displayed in Fig. 1–3. We attributed this higher reactivity to its significantly lower effective particle size, with DLS diameters below 10 nm versus 30–50 nm for the other particles and to higher Ce^{4+} on the surface. The effect of particle size on surface chemistry has already been reported for CNPs [28]. Decrease in nanoparticles size and increase in stability are directly related to increase in the active surface area for the reaction [9]. From the proposed reaction and XPS data it can be concluded that higher surface Ce^{4+} is necessary for better ClO^- scavenging. It is interesting to mention that CNP1 (73%) has a comparable amount of Ce^{4+} to that of CNP3 (70%) and similar nominal size (5–8 nm); however, CNP3 has the highest scavenging activity. Thus, lower stability of CNP1 (higher agglomeration, Table 1) contributed towards lower ClO^- scavenging activity. Noteworthy, CNP2, which also showed a minor surface interaction as revealed by absorption spectroscopy, had a surface composition very similar to that of CNP1. In conclusion, we determined that CNPs were able to scavenge ClO^- both in test tube and in vitro RAW cell culture model by surface interaction and a reaction involving the evolution of oxygen and the reduction of Ce^{4+} to Ce^{3+}. The results are relevant because HOCl/ClO^- is involved in tissue damage due to overstimulation of inflammatory processes.

Acknowledgements

This research was supported by the Ministry of Economy of Spain (CTM2013-45775-C2-1-R/2-R) and the Dirección General de Universidades e Investigación de la Comunidad de Madrid, Research Network S2013/MAE-2716. Dr Sueli de Oliveira Silva acknowledges Capacitação de Aperfeiçoamento de Pessoal de Nível Superior (CAPES)-Brazil for support. Gerardo Pulido-Reyes thanks the Spanish Ministry of Education for the award of a FPU grant.

References

1. A. A. Alfadda and R. M. Sallam, *J. Biomed. Biotechnol.*, 2012, **2012**, 936486.
2. L. J. Palmer, P. R. Cooper, M. R. Ling, H. J. Wright, A. Huissoon and I. L. C. Chapple, *Clin. Exp. Immunol.*, 2012, **167**, 261-268.
3. S. M. McKenna and K. J. Davies, *Biochem. J,* 1988, **254**, 685-692.
4. J. D. Imig and M. J. Ryan, *Compr. Physiol.*, John Wiley & Sons, Inc., 2013.
5. B. Bekdeser, N. Durusoy, M. Ozyurek, K. Guclu and R. Apak, *J. Agric. Food Chem*, 2014, **62**, 11109-11115.
6. O. Firuzi, P. Mladenka, R. Petrucci, G. Marrosu and L. Saso, *J. Pharm. Pharmacol.*, 2004, **56**, 801-807.
7. O. Firuzi, L. Giansanti, R. Vento, C. Seibert, R. Petrucci, G. Marrosu, R. Agostino and L. Saso, *J. Pharm. Pharmacol.*, 2003, **55**, 1021-1027.
8. J. Pedraza-Chaverri, G. Arriaga-Noblecia and O. N. Medina-Campos, *Phytother. Res.*, 2007, **21**, 884-888.

9. S. Das, J. M. Dowding, K. E. Klump, J. F. McGinnis, W. Self and S. Seal, *Nanomedicine*, 2013, **8**, 1483-1508.
10. F. Esch, S. Fabris, L. Zhou, T. Montini, C. Africh, P. Fornasiero, G. Comelli and R. Rosei, *Science*, 2005, **309**, 752-755.
11. E. G. Heckert, A. S. Karakoti, S. Seal and W. T. Self, *Biomaterials*, 2008, **29**, 2705-2709.
12. J. M. Dowding, T. Dosani, A. Kumar, S. Seal and W. T. Self, *Chem. Commun.*, 2012, **48**, 4896-4898.
13. J. Chen, S. Patil, S. Seal and J. F. McGinnis, *Nat. Nanotechnol.*, 2006, **1**, 142-150.
14. 2014 - US 8795731 B1.
15. S. Soren, S. R. Jena, L. Samanta and P. Parhi, *Appl. Biochem. Biotechnol.* 2015, **177**, 148-161.
16. S. Chigurupati, M. R. Mughal, E. Okun, S. Das, A. Kumar, M. McCaffery, S. Seal and M. P. Mattson, *Biomaterials*, 2013, **34**, 2194-2201.
17. Z. Liu, Y. Yan, S. Wang, W.-Y. Ong, C. N. Ong and D. Huang, *Am. J. Biomed. Sci*, 2013, **2**, 140-153.
18. S. Das, S. Singh, J. M. Dowding, S. Oommen, A. Kumar, T. X. Sayle, S. Saraf, C. R. Patra, N. E. Vlahakis, D. C. Sayle, W. T. Self and S. Seal, *Biomaterials*, 2012, **33**, 7746-7755.
19. T. Sakthivel, S. Das, A. Kumar, D. L. Reid, A. Gupta, D. C. Sayle and S. Seal, *ChemPlusChem*, 2013, **78**, 1446-1455.
20. A. Kumar, S. Das, P. Munusamy, W. Self, D. R. Baer, D. C. Sayle and S. Seal, *Environ. Sci.: Nano*, 2014, **1**, 516-532.
21. S. Deshpande, S. Patil, S. V. N. T. Kuchibhatla and S. Seal, *Appl. Phys. Lett.*, 2005, **87**, 133113.
22. O. I. Aruoma and B. Halliwell, *Biochem. J*, 1987, **248**, 973-976.
23. S. Shukla, A. Mehta, V. K. Bajpai and S. Shukla, *Food Chem. Toxicol.*, 2009, **47**, 2338-2343.
24. C. J. Neal, S. Das, S. Saraf, L. Tetard and S. Seal, *ChemPlusChem*, 2015, **80**, 1680-1690.
25. J. Zhang, X. Xu and X. Yang, *Analyst*, 2012, **137**, 3437-3440.
26. Y. Liu and L. Shen, *Langmuir*, 2008, **24**, 11625-11630.
27. S.-R. Liu, M. Vedamalai and S.-P. Wu, *Anal. Chim. Acta.*, 2013, **800**, 71-76.
28. S. V. Kuchibhatla, A. S. Karakoti, D. R. Baer, S. Samudrala, M. H. Engelhard, J. E. Amonette, S. Thevuthasan and S. Seal, *J. Phys. Chem. C.*, 2012, **116**, 14108-14114.

Electronic Supplementary Information:
DOI: 10.1039/x0xx00000x

Hypochlorite scavenging activity of cerium oxide nanoparticles

Gerardo Pulido-Reyes[1], Soumen Das[2], Francisco Leganés[1], Sueli O. Silva[3], Shu-Pao Wu[6], Francisca William Self[5], Fernández-Piñas[1], Roberto Rosal[6,*], Sudipta Seal[2,7,*]

1 Departamento de Biología, Facultad de Ciencias, Universidad Autónoma de Madrid, E-28049, Spain
2 Advanced Materials Processing and Analysis Center, NanoScience and Technology Center, Materials Science and Engineering, University of Central Florida, Orlando, FL 32816, USA
3 Departamento de Ciências Básicas da Saúde, Universidade Estadual de Maringá, 87020-900 Maringá, PR, Brazil.
4 Department of Applied Chemistry, National Chiao Tung University, Hsinchu, Taiwan 300, Republic of China.
5 Burnett School of Biomedical Science, College of Medicine, University of Central Florida, USA.
6 Departamento de Ingeniería Química, Universidad de Alcalá, E-28871, Alcalá de Henares, Madrid, Spain
7 College of Medicine, University of Central Florida, USA

* Corresponding authors: roberto.rosal@uah.es, sudipta.seal@ucf.edu

Experimental Section

1. Nanoparticles preparation and characterization

Synthesis of the nanoparticles were described in our previous publications. Briefly, CNP1 was synthesized using precipitation method. Cerium nitrate hexahydrate was dissolved in distilled water and equimolar mixture NH_4OH was used as oxidizer [1]. The solution was the stirred for 4 hours and particles were washed with distilled water for three times. CNP2 was prepared using hydrothermal method. Cerium nitrate hexahydrate was dissolve in water and then NaOH was added to adjust pH to 10. This solution were mixed properly in a Teflon bottle and subjected to hydrothermal treatment at 80° C for 6 h [2]. Then particles were washed with distilled water for three times. CNP3 was also prepared using precipitation method. Cerium nitrate hexahydrate was dissolved in distilled water and excess amount of NH_4OH was added. Then solution was stirred for 4 hours and washed with distilled water for three times. Pellet was resuspended in water and 1N HNO_3 was added to decrease the pH to 4 for better stability [3]. Lastly, CNP4 was prepared using wet chemical method, where equimolar H_2O_2 was used as oxidizer. 1N HNO_3 was used to decrease the pH to 4 for better stability [1].

These four nanoparticles were then thoroughly characterized. Size and morphology of the nanoparticles were analyzed using High Resolution Transmission Electron Microscopy (HRTEM). Surface charge and hydrodynamic radius of the nanoparticles were estimated using Zetasizer (Nano-ZS from Malvern Instruments, Houston, TX). X-ray photoelectron spectroscopy (5400 PHI ESCA; Mg KR X-ray irradiation (1253.6 eV) and 350 W) was used to determine the surface chemistry of the nanoparticles.

2. UV-Vis ClO^- absorption study

The interaction of CNP3 with ClO^- was revealed by UV-vis absorption spectrometry. A 10 mM stock solution of hypochlorite (ClO^-) was prepared immediately before the experiment. The reaction mixture contained, in a final volume of 1.5 ml, ClO^- (5 mM) and increasing concentrations (from 1 to 2.5 mM) of each CNPs (CNP3 and CNP2). After mixing both, the nanoparticles were centrifuged at 13000 rpm during 5 min and carefully washed three times with distilled water, in order to avoid the presence of free ClO^-. Finally, the absorption spectra (220-750 nm) were recorded using a Perkin Elmer Lambda 750S instrument.

3. Oxygen evolution measurements

Oxygen evolution was measured at 25°C under stirring (0.1 g) with a Clark-type oxygen electrode (Hansatech, Kings Lynn, UK). Firstly, 2 ml of distilled water were added to the chamber and dissolved oxygen was displaced with argon gas. Then, the chamber cap was opened and CNP3 or CNP4 at final concentration of 1 mM was added. Finally, the reaction mixture was completed when ClO^- (5 mM) was added. Oxygen evolution was tracked during 30 min. There was no evidence of oxygen release when nanoparticle or ClO^- alone was added (see supplementary figure S3).

4. ClO^- measurement in RAW cells

30×10^3 RAW cells/cover slips were seeded and then cultured overnight. Cells were then treated with two different concentrations of CNP3 (1 and 10 μM) and incubated for 6 h. After the incubation, 10 μM and 100 μM NaOCl were added to the culture and incubated 30 min for at 37 °C. Following washing with sterile saline solution, cells were treated with 2 μl of 10 mM HCS (HSC was provided by Dr. Shu-pao Wu) dissolved in DMSO and was incubated for 30 min at 37 °C. Finally, cells were washed with sterile saline and immediately, imaged under a confocal (Carl Zeiss confocal microscope with Volocity image processing software) microscope using 20x water immersion lenses and ten different regions were randomly imaged. Image J was used to get semi-quantitative data from the confocal images.

References

1. S. Das, S. Singh, J. M. Dowding, S. Oommen, A. Kumar, T. X. Sayle, S. Saraf, C. R. Patra, N. E. Vlahakis, D. C. Sayle, W. T. Self and S. Seal, *Biomaterials*, 2012, **33**, 7746-7755.
2. T. Sakthivel, S. Das, A. Kumar, D. L. Reid, A. Gupta, D. C. Sayle and S. Seal, *ChemPlusChem*, 2013, **78**, 1446-1455.
3. J. M. Dowding, T. Dosani, A. Kumar, S. Seal and W. T. Self, *Chemical communications*, 2012, **48**, 4896-4898.

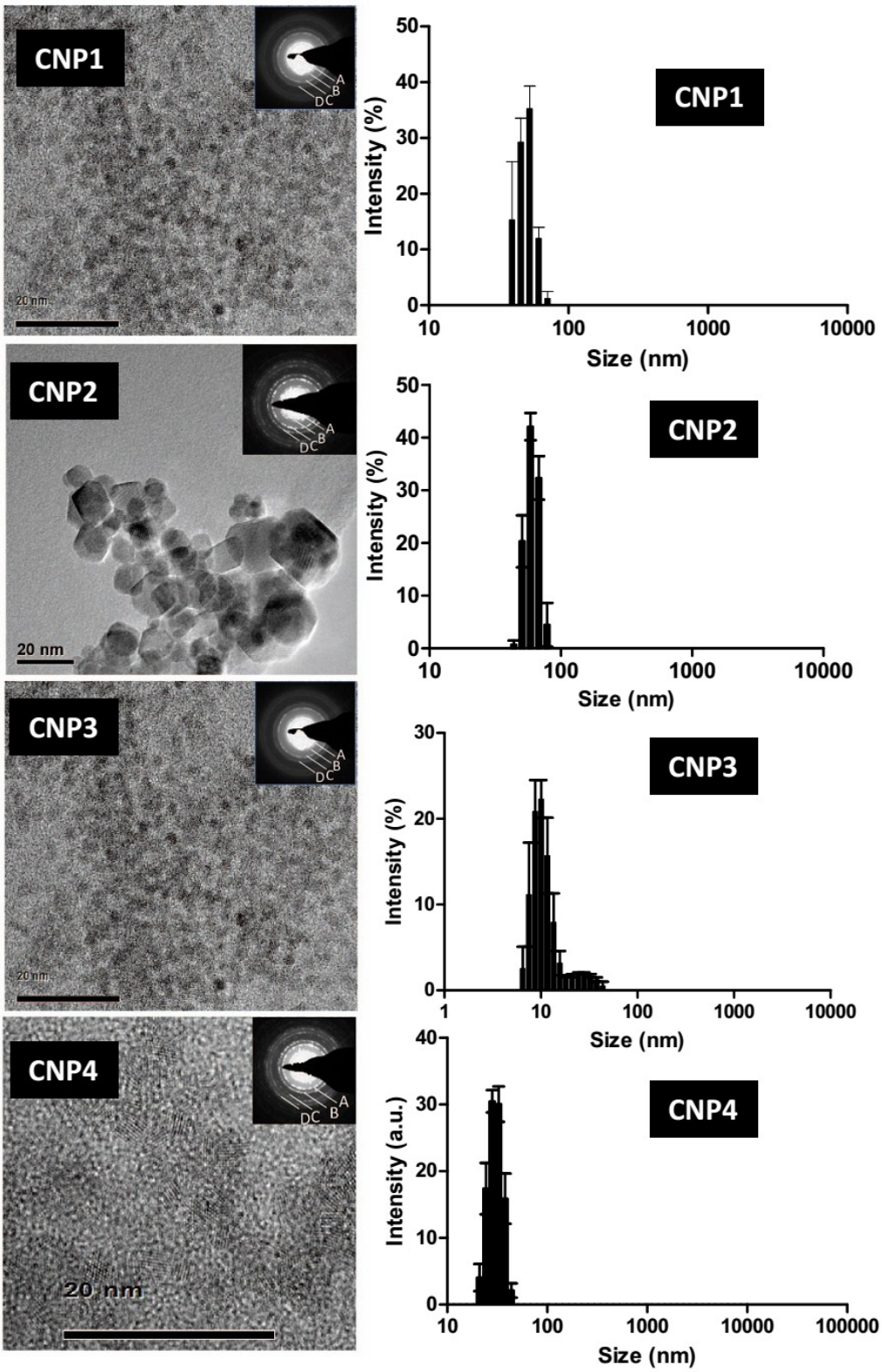

Figure S1. HRTEM images of CNPs show nanoparticles morphology (left panel) and the size distribution histogram using dynamic light scattering (DLS) (Left panel). The nominal sizes of the particles are as follows: CNP1 5-8 nm, CNP2 15-20 nm, CNP3 5-8 nm, CNP4 3-5 nm. Selected area electron diffraction patterns (SAED) of the particles are shown in the inset. SAED patterns confirm the crystalline nature and A(111), B(200), C(220) and D(311) are different lattice planes of CNPs fluorite crystal structure. Scale bars 20 nm. DLS data showed size of the different nanoparticles as follows: CNP1: 50.8 ± 0.9 nm; CNP2: 58.8 ± 0.8nm; CNP3: 9.4 ± 2.1 nm; CNP4: 30.8 ± 2.8 nm. The increase in the size of the nanoparticles is due to partial agglomeration of the nanoparticles.

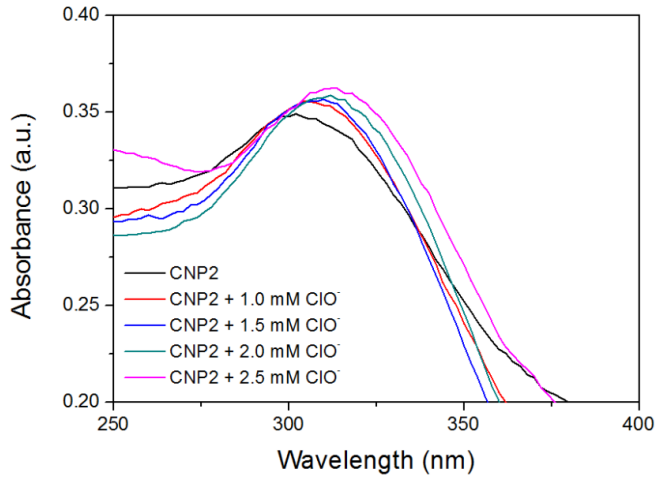

Figure S2. UV-vis spectra showing the interaction of CNP2 and ClO^-.

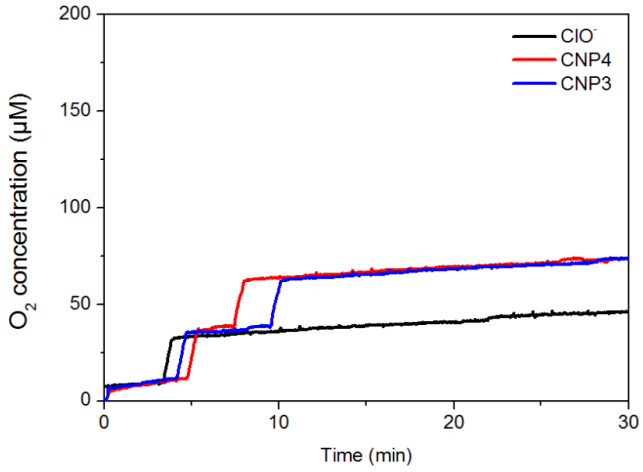

Figure S3. Oxygen evolution for CNP3, CNP4 and ClO^- alone, indicating that there was no evidence of oxygen release when nanoparticle or ClO^- alone was added.

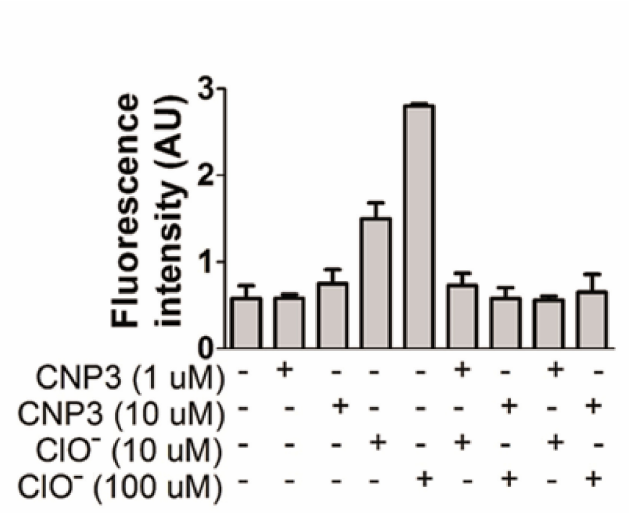

Figure S4. Semi-quantitative fluorescence intensity data of ClO^-. Data indicated ClO^- in CNP3 pretreated samples were comparable to control. CNP3 itself did not induce any ClO^-.